Measurement of Jupiter's asymmetric gravity field

Published Version:
Measurement of Jupiter's asymmetric gravity field / Iess, L.*; Folkner, W.M.; Durante, D.; Parisi, M.; Kaspi, Y.; Galanti, E.; Guillot, T.; Hubbard, W.B.; Stevenson, D.J.; Anderson, J.D.; Buccino, D.R.; Casajus, L. Gomez; Milani, A.; Park, R.; Racioppa, P.; Serra, D.; Tortora, P.; Zannoni, M.; Cao, H.; Helled, R.; Lunine, J.I.; Miguel, Y.; Militzer, B.; Wahl, S.; Connerney, J.E.P.; Levin, S.M.; Bolton, S.J.. - In: NATURE. - ISSN 0028-0836. - STAMPA. - 555:7695(2018), pp. 220-222. [10.1038/nature25776]

Availability:
This version is available at: https://hdl.handle.net/11585/632494 since: 2018-03-28

Published:
DOI: http://doi.org/10.1038/nature25776

The measurement of Jupiter's asymmetric gravity field

L. Iess[1*], W.M. Folkner[2], D. Durante[1], M. Parisi[2], Y. Kaspi[3], E.Galanti[3], T. Guillot[4], W. B. Hubbard[5], D.J. Stevenson[6], J.D. Anderson[7], D. R. Buccino[2], L. Gomez Casajus[8], A. Milani[9], R. Park[2], P. Racioppa[1], D. Serra[9], P. Tortora[8], M. Zannoni[8], H. Cao[6], R. Helled[10], J.I. Lunine[11], Y. Miguel[4], B. Militzer[12], S. Wahl[12], J.E.P. Connerney[13], S.M. Levin[2], S.J. Bolton[7]

[1]*Sapienza Università di Roma, 00184 Rome, Italy*

[2]*Jet Propulsion Laboratory/Caltech, Pasadena, CA 91109, USA*

[3]*Weizmann Institute of Science, Rehovot 76100, Israel*

[4]*Observatoire de la Côte d'Azur, 06304 Nice, France.*

[5]*Lunar and Planetary Laboratory, University of Arizona, Tucson, AZ 85721, USA*

[6]*California Institute of Technology, Pasadena, CA 91125, USA.*

[7]*Southwest Research Institute, San Antonio, TX 78238, USA*

[8]*Università di Bologna, 47100 Forlì, Italy*

[9]*Università di Pisa, 56127 Pisa, Italy*

[10]*University of Zurich, 8057 Zurich, Switzerland*

[11]*Cornell University, Ithaca, NY 14853, USA*

[12]*University of California, Berkeley, CA 94720, USA*

[13]*NASA Goddard Space Flight Center, Greenbelt, MD 20771, USA*

[*]Corresponding author. Email: luciano.iess@uniroma1.it

The gravity harmonics of an oblate rotating planet can be decomposed into static components (arising from solid body rotation) and dynamic components. Within the framework of models of the gas giant planets, even zonal components J_{2n} **are approximately proportional to** q^n**, where** q **is the ratio between centrifugal acceleration and gravity at the equator**[1]**. Any asymmetry in the gravity field is attributed to differential rotation and deep atmospheric flows. The odd harmonics,** J_3, J_5, J_7, J_9 **and higher, are a measure of the depth of the winds in the different zones of the atmosphere**[2,3]**. Here we report measurements of Jupiter's gravity harmonics (both even and odd) through precise Doppler tracking of the Juno spacecraft in its polar orbit around Jupiter. We find a north-south asymmetry, which is the signature of atmospheric and interior flows. The analysis of the harmonics is done in two companion papers**[4,5].

The external, harmonic, gravitational potential of a body can be expanded in a series of complex spherical harmonic functions $\boldsymbol{Y_{lm}(\theta, \varphi)}$ (an orthonormal basis for functions defined on the unit sphere) multiplied by a scaling factor depending on a normalized radial distance r/R

$$U(r,\theta,\varphi) = -\frac{GM}{r}\left[1 + \sum_{l\geq 2}\left(\frac{R}{r}\right)^{l+1}\sum_{m=-l}^{l} U_{lm}Y_{lm}(\theta,\varphi)\right]$$

For a planet, R is generally chosen as the equatorial radius of the body. Were the internal density ρ of the body known, the harmonic coefficients U_{lm} could be obtained from the integral over the volume V of the body[6]

$$U_{lm} = \frac{1}{(2l+1)MR^l}\int_V r'^l\, Y_{lm}(\theta',\varphi')\rho(r',\theta',\varphi')dV'$$

When the density does not depend on longitude, as expected for a fluid and rapidly rotating planet like Jupiter, the above expression simplifies in

$$J_l \equiv -U_{l0} = -\frac{1}{(2l+1)MR^l} \int_V r'^l \, P_l(\theta')\rho(r',\theta')dV'$$

where P_l is the Legendre polynomial of degree l. Thus, zonal coefficients J_l bear important, although non-unique, information on the density distribution inside Jupiter.

On July 4, 2016 the Juno spacecraft was captured by the gravity field of Jupiter, starting its prime mission devoted to the investigation of the deep interior, the magnetosphere, and the atmosphere of the planet. The spacecraft is currently in a highly eccentric (e=0.98), long period (52.9 days), polar orbit, with a pericenter altitude of about 4000 km above the 1 bar level as inferred from radio occultations[7].

As a consequence of the equivalence principle, gravity field determinations require the measurement of the relative motion between (at least) two masses. In the Juno gravity experiment, the spacecraft acts as a test particle falling in the gravity field of the planet. The Earth is the second end mass. Jupiter's gravity is inferred from range rate measurements between a ground antenna and the spacecraft during pericenter passes. In Juno gravity determinations, the ground station transmits two carriers, respectively at 7,153 MHz (X-band) and 34,315 MHz (Ka band). Onboard, a X band transponder and a dedicated Ka band frequency translator (a radio science instrument) lock the incoming carriers and retransmit them back to ground at 8,404 MHz and 32,088 MHz. The range rate (Doppler) observable is obtained by comparing the transmitted and received frequencies. Juno is the first deep space mission using Ka band radio systems for planetary geodesy. Ka band and multifrequency radio links were previously employed only for precision tests of relativistic gravity with the Cassini spacecraft in the cruise phase[8,9]. Due to the dispersion properties of plasmas, Ka band radio links provide excellent immunity to the adverse effects of charged particles along the propagation path, including the Io torus (a potential source of bias in the gravity estimates[10]). The Juno radio system enables a further reduction of plasma noise (approximately 75%) by combining X and Ka band Doppler observables[11]. In order to reduce the noise from tropospheric water vapour, a radiometer placed near the ground antenna was continuously monitoring the wet path delay along the line of sight.

Our analysis is based on the first two Ka band gravity passes of Juno, labelled PJ3 (11 December 2016) and PJ6 (19 May 2017). Doppler measurements were integrated over 60 s prior to processing in order to enable adequate sampling of the gravity signal. At this time scale the measured two-way range rate noise at Ka band was $2x10^{-5}$ m/s at 60 s, in line with the expectations from Ka band radio link noise models[12]. The Doppler noise is approximately white between $4x10^{-4}$ and $2x10^{-2}$ Hz (the characteristic frequency range of the gravity signal).

The dynamical model used in the orbital fit is driven by the theoretical expectations for the gravity field of gaseous planets. We adopt here the standard spherical harmonics representation of planetary gravity fields, whose expansion coefficients are determined by the density distribution inside the body[6]. Models of the interior structure predict that Jupiter's gravity is dominated by an axially and hemispherically symmetric component due to solid body rotation[13,14]. This component is determined by the radial density distribution in the rotating planet and is represented by even zonal harmonic coefficients $J_{2n}{\sim}q^n$. Atmospheric and internal dynamics can produce small density perturbations that result in a more complex gravity representation, involving odd zonal and possibly tesseral harmonics, as well as small corrections to the even zonal harmonics[3,5,15]. The latter are however indiscernible from the much larger contribution of solid body rotation up to harmonics of degree 12, where the dynamics is expected to lead the gravity signal[2]. Hence, any detection of an asymmetric (hemispherically or axially) gravity field would be a unique indication of internal dynamics due to flows. Juno tracking data have provided the first ever evidence of hemispherical (North-South) asymmetries in the gravity field of a giant planet.

Prior to PJ3, the best determination of Jupiter's even zonal gravity field was carried out using lower quality Doppler observables from the first two Juno pericenter passes (PJ1 and PJ2)[16,17]. These early results improved previous determinations of the zonal harmonic coefficients J_4 and J_6[18,19] and allowed the first determination of J_8. Those measurements of J_4 and J_6 have been used to constrain the radial density profile of the planet[20]. However, the magnitude of the much smaller odd zonal field could not be determined, because of the unfavourable observation geometry and the large propagation noise caused by the interplanetary plasma on the X band uplink (7.2 GHz).

High accuracy Ka band data acquired during PJ3 and PJ6 provided the first determination of the asymmetric component of Jupiter's gravity (Fig. 1 and Table 1). We processed Doppler data using orbit determination codes developed for spacecraft navigation (JPL software MONTE) and an external estimation filter. Data from PJ3 and PJ6 were separately fitted for the spacecraft state vector at the beginning of the tracking pass (about 6 h prior to transit at pericenter), Jupiter's gravitational parameter GM, the zonal harmonic coefficients J_2-J_{24}, the tesseral quadrupole harmonics, the pole position and rate at epoch J2017.0, and the k_{22} Love number. This set of parameters allows fitting all data to the noise level. The l=2 tesseral coefficients, although not strictly required by a least size solution, have been estimated to search for a possible deviation of the principal axis of inertia from the spin axis. The masses and the ephemerides of the Jovian satellites are adopted from JUP 310[19] and not estimated, although their uncertainties have been considered in the final covariance matrix. A linear correction to the orbit of Jupiter was applied in order to fit range data acquired at X band during the tracking pass. The relativistic Lense-Thirring precession is included, and the magnitude of Jupiter's polar moment of inertia set to interior model predictions, considered with a 20% of uncertainty (affecting the recovery of Jupiter's spin axis). The single-arc solutions were then combined in a global multi-arc solution made up by two categories of parameters: local (pertaining to each arc) and global (common to both arcs). Only spacecraft initial conditions are treated as local parameters. No constraints have been applied to the global parameters except Jupiter's GM, whose current estimate is more accurate than that obtained so far from Juno[10]. The data are weighted according to the Doppler noise in each Ka band pass, assuming no correlation between samples. The correctness of this assumption is verified a posteriori from the nearly white power spectral density of the residuals in the frequency band of interest[10].

The two single-arc gravity solutions are fully compatible at 2σ except J_4 (3.5σ; see Fig. 2 for some examples). Fitting jointly PJ3 and PJ6 data does not require any tesseral component other than the quadrupole, even if the two ground tracks are separated by about 150°. However, available data do not allow setting a reliable upper limit to tesseral harmonics, although numerical simulations indicate that a tesseral field corresponding to a flow depth larger than 380 km would produce signatures in the Doppler residuals[10,21]. Consider covariances corresponding to this flow depth are larger than the uncertainties reported in Table 1[10]. The current data set does not show evidence of a time-varying gravity field, as may result from Jupiter's normal modes[22].

Since for large-scale flows on rotating planets wind shear is accompanied by density gradients, it is possible to directly link the flows and the gravity field. The velocity gradient affects both the even and odd zonal harmonic coefficients, but only the odd coefficients bear the unique signature of the dynamics when l<10 (for l>10 also the even coefficients are dominated by the dynamics of the flows - see Fig. 1). We singled out the contribution of the winds by removing the J_2, J_4, J_6, J_8 harmonic components from the complete gravity potential. The North-South asymmetric component of the gravity acceleration reaches the largest magnitude of 3.4±0.4 mGal (3σ) at a latitude of 24°N, approximately at the transition between the Northern Equatorial Belt and the Northern Tropical Zone (Fig. 3). Remarkably, this region corresponds to a large velocity and latitudinal gradient of surface winds, as expected for a gravity signal due to wind dynamics[4,15]. The odd zonal harmonics J_3, J_5, J_7, J_9 and the associated gravity acceleration may be used to infer the depth and the vertical profile of the winds[3,4].

References

1. Lanzano, P. The equilibrium of a rotating body of arbitrary density. *Astrophys. Space Sci.* 29, 161-178 (1974).
2. Hubbard, W. B. Note: Gravitational signature of Jupiter's deep zonal flows. Icarus 137, 357–359 (1999).
3. Kaspi, Y. Inferring the depth of the zonal jets on Jupiter and Saturn from odd gravity harmonics. *Geophys. Res. Lett.* **40**, 676–680 (2013).
4. Kaspi, Y., et al. Jupiter's deep atmosphere revealed by Juno's asymmetric gravity measurements, *Nature* (2018), this issue.
5. Guillot, T., et al. Suppressed differential rotation in Jupiter's deep interior, *Nature* (2018), this issue.
6. Bertotti, B., Farinella, P., & Vokrouhlicky, D. (2012). Physics of the solar system: dynamics and evolution, space physics, and spacetime structure, p. 45, Springer (2012), with earlier references therein.
7. Lindal, G. F., et al. The atmosphere of Jupiter: An analysis of the Voyager radio occultation measurements. *J. Geophys. Res.* **86**, 8721-8727 (1981).
8. Bertotti, B., L. Iess, and P. Tortora A test of general relativity using radio links with the Cassini spacecraft. *Nature* **425**, 374-376 (2003).

9. Armstrong, J.W., Iess, L., Tortora, P. & Bertotti, B. Stochastic gravitational wave background: upper limits in the 10-6-10-3 Hz band. *Astrophys. J.*, **599**, 806-813 (2003).

10. See Methods section.

11. Bertotti, B., Comoretto, G. & Iess, L. Doppler tracking of spacecraft with multifrequency links. *Astron. Astrophys.* **269**, 608-616 (1993).

12. Asmar, S. W., Armstrong, J. W., Iess, L. & Tortora. P. Spacecraft Doppler tracking: Noise budget and accuracy achievable in precision radio science observations. *Radio Science* **40**(2) (2004).

13. Hubbard, W. B. Effects of differential rotation on the gravitational figures of Jupiter and Saturn. *Icarus*, **52**, 509–515 (1982).

14. Hubbard, W. B. & Militzer, B. A preliminary Jupiter model. *Astrophys. J.*, **820**, 80-93 (2016).

15. Kaspi, Y., Hubbard, W. B., Showman, A. P. & Flierl, G. R. Gravitational signature of Jupiter's internal dynamics. *Geophys. Res. Lett.* **37**, L01204 (2010).

16. Bolton, S. J., et al. Jupiter's interior and deep atmosphere: The initial pole-to-pole passes with the Juno spacecraft. *Science* **356**(6340), 821-825 (2017).

17. Folkner, W. M., et al. Jupiter gravity field estimated from the first two Juno orbits. *Geophysical Research Letters* **44** (2017) doi:10.1002/2017GL073140.

18. Jacobson, R., Haw, R., McElrath T. & Antreasian P. A comprehensive orbit reconstruction for the Galileo prime mission. *Adv. Astronaut. Sci.*, **103**, 465–486. (1999),

19. Jacobson, R. A. Jupiter satellite ephemeris file Jup310, NASA Navigation and Ancillary Information Facility. (2009), [Available at https://naif.jpl.nasa.gov/pub/naif/generic_kernels/spk/satellites/jup310.bsp]

20. Wahl, S. M. *et al.* Comparing Jupiter interior structure models to Juno gravity measurements and the role of an expanded core. *Geophys. Res. Lett.* **44**, 4649–4659 (2017).

21. Parisi, M., et al. Probing the depth of Jupiter's Great Red Spot with the Juno gravity experiment. *Icarus* **267,** 232-242 (2016).

22. Durante, D., Guillot, T. & Iess, L. The effect of Jupiter oscillations on Juno gravity measurements. *Icarus* **282**, 174-182 (2017).

Acknowledgments

The research described in this paper was carried out at the Sapienza University of Rome, University of Bologna, and University of Pisa under the sponsorship of the Italian Space Agency; at the Jet Propulsion Laboratory, California Institute of Technology, under a contract with the NASA; by the Southwest Research Institute under contract with the NASA. Support was provided also by the Israeli Space Agency (YK and EG), and CNES (TG and YM). All authors acknowledge support from the Juno Project. The data used in this paper will be available through the NASA Planetary Data System.

Author contributions

L.I. and W.F. led the experiment and supervised the data analysis. L.I. wrote most of the manuscript. D.D. and M.P. carried out the gravity data analysis. Y.K. and E.G. provided models of the asymmetric and tesseral gravity field. Y.K., E.G., T.G., W.H., and D.J.S. carried out consistency checks with interior models and provided theoretical support. D.R.B. planned and supervised the data collection. P.R. designed and coded the orbit determination filter used in this analysis. L.C., P.T., and M.Z. provided the media calibrations. J.D.A., A.M., R.P., and D.S. advised in the data analysis. H.C., R.H., J.I.L., Y.M., B.M., and S.W. helped in the definition of the scientific objectives of the measurements. J.E.P.C., S.M.L., S.J.B. supervised the planning, execution, and definition of the gravity experiment.

Author Information. The authors declare that they have no competing financial interests. See npg.nature.com/reprintsandpermissions for reprints and permissions information. Correspondence and requests for materials should be addressed to L. Iess (email: luciano.iess@uniroma1.it).

Table 1. Gravity solution

	Value	Uncertainty
J_2 (x10^6)	14696.572	0.014
C_{21} (x10^6)	-0.013	0.015
S_{21} (x10^6)	-0.003	0.026
C_{22} (x10^6)	0.000	0.008
S_{22} (x10^6)	0.000	0.011
J_3 (x10^6)	-0.042	0.010
J_4 (x10^6)	-586.609	0.004
J_5 (x10^6)	-0.069	0.008
J_6 (x10^6)	34.198	0.009
J_7 (x10^6)	0.124	0.017
J_8 (x10^6)	-2.426	0.025
J_9 (x10^6)	-0.106	0.044
J_{10} (x10^6)	0.172	0.069
J_{11} (x10^6)	0.033	0.112
J_{12} (x10^6)	0.047	0.178
k_{22}	0.625	0.063
RA (deg)	268.0570	0.0013
Dec (deg)	64.4973	0.0014

Legends

Table 1. **Gravity solution**. Jupiter's gravity harmonics coefficients (un-normalised; reference radius = 71492 km), Love number k_{22}, pole coordinates at epoch J2017.0, obtained from PJ3 and PJ6 Juno science orbits. The deviation of the principal axis of inertia from the spin axis, as inferred from the uncertainty in C_{21} and S_{21}, is bound to be less than about 0.4 arcsec (130 m at the reference radius). J_2 includes a tidal term currently estimated at ~2.98 10^{-8}. The associated uncertainties are realistic values to be used for analysis and interpretation. They correspond to three times the formal 1σ uncertainties.

Fig. 1. Zonal gravity harmonic coefficients J_2-J_{12}. The dashed line shows the realistic uncertainty (Tab. 1). Positive and negative values are respectively in solid and empty circles.

Fig. 2. 3-σ uncertainty ellipses of J_3-J_5 **and** J_7-J_9. Brown and cyan ellipses refer respectively to single arc PJ3 and PJ6 solutions. The solid violet ellipse refers to the PJ3+PJ6 combined solution.

Fig. 3. Gravity disturbances due to wind dynamics. Latitudinal dependence of residual gravity acceleration (in mGal, positive outwards) and associated 3σ uncertainty (shaded area) at a reference distance of 71492 km, when gravity from even zonal harmonics J_2, J_4, J_6 and J_8 is removed. The residual gravity field, dominated by the dynamics of the flows, shows marked peaks correlated with the band structure. The latitudinal gradient of the measured wind profile is shown in the right panel. The largest (negative) peak of -3.4±0.4 mGal (3σ) is found at a latitude of 24°N, where the latitudinal gradient of the wind speed reaches its largest value. The relation between the gravity disturbances and wind gradients is discussed in a companion paper[4].

Methods

Data acquisition. Previous determinations of the Jovian gravity with Juno were carried out by means of the standard radio system of the spacecraft at X band (7.2-8.4 GHz) during the first two pericenter passes (PJ1 and PJ2). At these lower frequencies Doppler data were marred by interplanetary plasma noise (although antenna mechanical noise was an important noise source in PJ1). Our analysis is based on radio tracking of Juno at Ka band during two pericenter transits on 11 December 2016 (17:03:40 UTC – PJ3) and 19 May 2017 (06:00:45 UTC – PJ6). The use of Ka band provided an excellent immunity to propagation noises due to charged particles. In the overall planning of the mission, PJ3 and PJ6 were the first two pericenter passes devoted to gravity science. Ground support was provided by DSS 25 (Goldstone, California), the only antenna of NASA's Deep Space Network (DSN) with two-way Ka band capabilities. Two-way Ka and X band data were acquired from 12:47 UTC to 19:19 UTC during PJ3 (about 390 Doppler observables points at 60 s for each band), and from 01:39 UTC to 09:25 UTC (about 460 Doppler observables per band) in PJ6. In order to improve the determination of the spacecraft trajectory, we have used also data acquired in X band from an antenna of the Canberra DSN complex (DSS 43) after the end of the DSS 25 pass, prior an orbit trimming manoeuver.

Doppler data were obtained from a wide band open loop receiver used for radio science investigations. A specially designed digital phase-locked loop has been applied to the 1 kHz complex samples of the received electric field to obtain the phase history and the sky frequencies. Doppler data from the standard closed loop receiver are generally noisier, thus resulting in larger formal uncertainties. Central values of the estimates from the two data sets are statistically compatible.

Non-gravitational accelerations. The dynamical model used in the fit is purely deterministic. All non-gravitational forces acting on the spacecraft are modelled by means of a suitable set of parameters, whose uncertainties contribute to the final covariance matrix. The largest non-gravitational acceleration is due to the solar radiation pressure (about 9×10^{-9} m/s^2) acting on the 61 m^2 solar panels and the 3 m high gain antenna. Its modelling is simple, as the sun aspect angle, therefore also the acceleration, is constant during the pass. We have assumed that the reflectivity of the surfaces is known with a 20% uncertainty. Our dynamical model includes also the small acceleration from the latitudinally varying, Jovian infrared emission (1.2×10^{-9} m/s^2 at the equator) and the radiation pressure from the albedo of the planet (6×10^{-10} m/s^2). The negligible effect on the gravity estimate due to inaccurate modelling on these non-gravitational accelerations has been again assessed by means of numerical simulations. The anisotropic thermal emission from the spacecraft and possible gas leaks may produce small, additional, accelerations along the direction of the spin axis (the other components being averaged out). As the direction of the Earth and the Sun differ by only 9° during the observations, these accelerations are confused with the solar radiation pressure and their effect in the estimate is accounted for in the 20% uncertainty attributed to solar radiation pressure. Other accelerations, such as atmospheric and magnetic drag, are too small to affect the gravity estimate.

Orbit geometry. The orbit geometry is a crucial factor in gravity determinations. The key parameters are the orbital altitude and the angle between the line of sight and the spacecraft acceleration. Juno’s pericenter altitudes are sufficiently low (4154 km in PJ3 and 3503 km in PJ6) to reveal density inhomogeneities with spatial scales much smaller than the radius of the planet. On the other hand, the large eccentricity causes the radial distance from the planet to increase quickly with latitude, strongly reducing the sensitivity to gravity disturbances in the polar regions (more markedly in the southern hemisphere, due to the location of the pericenter north of the equator). The eccentricity of the orbit limits also the gravitational contact time: the spacecraft covers 60 degrees in latitude in about 1200 s, reaching a velocity of about 60 km/s at pericenter. The other factor affecting the recovery of the gravity field is the orientation of the orbital plane with respect to Earth, which controls the projection of the spacecraft velocity along the line of sight. Although the angle between the opposite to the orbit normal and the Earth direction is not optimal (19.2° in PJ3 and 15.1° in PJ6), the projected velocity and acceleration still provide good observability of the zonal field.

The pericenter latitude undergoes secular variations due to Jupiter's oblateness, allowing a more complete coverage of Jupiter's gravity. The pericenter drifts northward by about 1° per orbit from an initial latitude of 2.7°. At the end of the nominal mission it will reach a latitude of 32.6°N, allowing a better determination of gravity at high northern latitudes. The node longitude is controlled by means of orbital manoeuvres to target specific Jupiter longitudes and obtain a uniform coverage. These manoeuvres are carried out far from pericenter and therefore do not affect the gravity determinations. The orientation of the orbital plane with respect to Earth changes from a nearly face-on configuration at orbit insertion to edge-on after about three years. Detailed information on Juno's orbit can be obtained from NASA's HORIZONS system[23]. Extended Data Table 1 reports the main geometrical parameters relevant to gravity determination.

Data quality and calibration. We have carefully assessed and ruled out significant biases in the gravity estimate due to systematic effects in the data and the dynamical model. The largest systematic effect in Doppler measurement is due to the dry troposphere, which causes path delay variations up to ≈ 3 x 10^{-4} m/s over time scales of 6-8 hours. The suppression of this large signal is obtained using ground meteorological data (mostly surface pressure and temperature) and a careful modelling of elevation-dependent effects. Although a small residual tropospheric signal (mostly due to horizontal pressure gradients) cannot be excluded, its time scale is much longer than that from the gravity harmonics (10-30 minutes). Its effect on the gravity determination is therefore negligible.

The path delay due to the ionospheric plasma is strongly reduced thanks to the use of Ka-band. The Deep Space Network provides anyway calibrations of the ionospheric path delays at each tracking complex by mapping dual frequency GPS measurements onto the spacecraft line of sight. The applied corrections never exceed a few centimetres over time scales of several hours, corresponding to path delay rates of ≈ 2 x 10^{-6} m/s. Although inherently small, these effects can be further reduced thanks to GPS-based calibrations.

According to models of Doppler noise in Ka-band interplanetary radio links[12], solar wind turbulence becomes a dominant noise source only at solar elongation angles lower than 15° when partial calibration aided by the X-band radio link is available[11,24]. For Juno the expected interplanetary plasma noise in PJ3 (elongation = 61.6°) and PJ6 (elongation = 135.4°) is respectively 3×10^{-7} m/s and 1×10^{-7} m/s at 60 s integration times. These values are well below the contributions expected from wet troposphere and antenna mechanical noise[12]. Path delay variations due to tropospheric water vapour were calibrated using two microwave radiometers located near the ground antenna, with parallel lines of sight. After calibrations, Doppler residuals integrated over 60 s were reduced by about 30%.

The relevant time scale of gravity measurements is determined by the spatial scale of the gravity field and by the spacecraft velocity. For the gravity harmonic of degree l, the time scale is roughly $\pi R_J / l\, V_{sc}$, where R_J is Jupiter's equatorial radius and V_{sc} is the spacecraft velocity near pericenter. For l=12, the time scale of the gravity signal is about 300 s. Doppler measurements were integrated over 60 s prior to processing in order to enable adequate sampling of the gravity signal. At this time scale the measured range rate noise at Ka band was 2×10^{-5} m/s at 60 s, in line with the expectations from Ka band radio link noise models[12]. The PJ3 and PJ6 Doppler residuals after plasma and tropospheric calibrations, and the corresponding Allan deviations are shown in Extended Data Fig. 1 and 2. The slope of the Allan deviation (approximately proportional to the inverse square root of the integration time) is consistent with a white Doppler noise between $4\text{x}10^{-4}$ and $2\text{x}10^{-2}$ Hz (the band of the gravity signal). The low Doppler noise experienced by Juno is much smaller than the gravity signal from the odd harmonics (example in Extended Data Fig. 3), facilitating their identification.

Effect of the Io plasma torus. Juno's radio signal invariably crosses the region of charged particles generated by the ionization of the gases emitted by Io's volcanos, known as the Io torus. The resulting path delay variation is a potentially important source of bias in the gravity estimates. The plasma density of the Io torus shows a variability of a factor of 2 over time scales of 20 days and is difficult to model[25]. The path delay variation during a Juno pass can be estimated and partially calibrated by means of differential Doppler measurements in the X and Ka band. In PJ3 and PJ6 we measured path delay variations ascribed to the Io torus of about 2-4 cm at Ka band over a time scale of about two hours (16 times larger at X band).

The fractional frequency shift y of the received signal can be modelled as the sum of a non-dispersive contribution y_{ND} (dominated by the orbital dynamics) and a dispersive contribution due to charged particles:

$$y = y_{ND} + k\left(\frac{\dot{P}_U}{f_U^2} + \frac{\dot{P}_D}{\alpha^2 f_U^2} + \frac{\dot{I}_U}{f_U^2} + \frac{\dot{I}_D}{\alpha^2 f_U^2}\right) \qquad (1)$$

Here f_U is the frequency of the signal transmitted by the ground station, α is the transponding ratio (the ratio between the frequency transmitted and received by the spacecraft), $\dot{P}_U$, $\dot{P}_D$, $\dot{I}_U$, and $\dot{I}_D$ are the time derivatives of the columnar electron content (TEC) from the interplanetary and ionospheric plasma (P), and Io torus (I), respectively in the uplink (U) and downlink (D) path. The constant $k = e^2/(8\pi^2\varepsilon_0 m_e c)$ is approximately 1.34x10^{-7} m^2/s. When multiple frequencies are available, the dispersive terms can be fully or partially measured thanks to the frequency dependence of the plasma refractive index[11,24].

Due to the difference in the X and Ka band transponding ratios (respectively 880/749 and 3360/3599), in PJ3 and PJ6 the overall plasma contribution can be estimated to a 75% accuracy[11]. Under the assumption $\dot{I}_U = \dot{I}_D$ (well verified because the Io torus is just within 1.5 light-seconds from Juno), the frequency shift due to the Io torus is obtained by differencing the X and Ka band relative frequency shift described by Eq. 1:

$$k\left(\frac{1}{f_K^2}+\frac{1}{\alpha_K^2 f_K^2}\right)\dot{I} = \left(\frac{f_K^2}{f_X^2}\frac{\alpha_K^2}{\alpha_X^2}\frac{\alpha_X^2+1}{\alpha_K^2+1}-1\right)^{-1}\left\{y_X - y_K - k\left[\dot{P}_U\left(\frac{1}{f_X^2}-\frac{1}{f_K^2}\right)+\dot{P}_D\left(\frac{1}{\alpha_X^2 f_X^2}-\frac{1}{\alpha_K^2 f_K^2}\right)\right]\right\} \quad (2)$$

In Eq. 2, the estimated Io torus signal is contaminated by the uplink and downlink interplanetary plasma TEC variations. In PJ3 and PJ6 data we observed a residual plasma noise of about 8x10^{-7} m/s (relative frequency shift 2.7x10^{-15}) at 60 s integration time. We have assessed the effect of this error by means of numerical simulations.

Simulated Doppler observables of PJ3 and PJ6 were generated using the same dynamical model adopted in the analysis of PJ3 and PJ6 data. A white Gaussian noise with a standard deviation equal to the observed one was added to the simulated observables. Then, we have added a signal mimicking the effect of the Io torus to the simulated Doppler observables using a simple Gaussian model for the path delay Δl on a signal of frequency f:

$$\Delta l = \Delta l_K\left(\frac{f_K}{f}\right)^2 \exp\left[-\frac{1}{2}\left(\frac{t-\Delta\tau}{\tau/6}\right)^2\right] \quad (3)$$

Here Δl_K is the maximum path delay on a signal with frequency f_K, τ is the total duration of the torus signal (corresponding to 6 standard deviation of a Gaussian curve), and $\Delta\tau$ is the delay between the time of maximum path delay and the orbit pericenter. The values of the parameters adopted for each flyby were derived from direct measurements carried out in PJ3 and PJ6. $\Delta l_K = (2.1;\ 4.6)$ cm, $\tau = (120;\ 150)$ min, $\Delta\tau = (-15;\ +10)$ min provide a good match to PJ3 and PJ6 observations, respectively. The fractional frequency shift Δy on the Doppler observables is given by:

$$\Delta y = \frac{\dot{\Delta l}}{c} = -\left(\frac{f_X}{f}\right)^2 \frac{\Delta l_K}{c\,\tau/6}\frac{t-\Delta\tau}{\tau/6}\exp\left[-\frac{1}{2}\left(\frac{t-\Delta\tau}{\tau/6}\right)^2\right] \qquad (.4)$$

To simulate the calibration error due to the residual plasma noise in Eq. 2, the calibrations were generated using the same model, but perturbing the input parameters with white, Gaussian random values. The standard deviations of the perturbing terms were chosen in order to match the observed solar plasma noise. The resulting standard deviation of the path delay δ is less than 10% of its value.

We then carried out a Monte Carlo simulation using 1000 noise realisations and obtained a sample of estimated gravity fields. None of the gravity harmonic coefficients changes by more than 1σ (see Extended Data Fig. 4 and 5 for examples). On the contrary, the Io torus can cause biases up to about 5σ on gravity solutions based on X band data. The most affected gravity coefficients are J_2, J_3, and J_4.

Tesseral gravity field. The solution reported in Table 1 includes only degree 2 tesseral gravity harmonics. Although higher degree tesseral harmonics are not required to fit the data to the noise level, a higher degree field is certainly present. In order to assess the effect of a tesseral field on the actual estimate, simulations with synthetic Doppler data have been conducted. Thermal winds models with a scale height of 1900 km, consistent with the observed odd harmonics[3] but with a different scale height for the vortices (associated to the tesseral component) have been used to generate synthetic gravity fields. The resulting simulated Doppler observables have been fitted with the dynamical model used to obtain our solution (Table 1), limited to degree 2 tesseral harmonics. Our goal is to identify the largest tesseral field (therefore the largest scale height) that can be hidden in the Doppler data without producing signatures in the residuals. We found that the threshold value of the scale height is about 380 km.

To include the effect of the neglected tesseral field in the estimation, a consider analysis has been performed. The consider analysis quantifies the effect of non-estimated parameters (the higher degree tesseral field) on the uncertainties of the estimated parameters. The effect on the estimate is an increase in the uncertainties. Extended Data Table 2 reports the consider uncertainties of the estimate for a thermal wind model having a scale height of the vortices of 380 km.

Data availability

The Juno tracking data and the ancillary information used in this analysis are archived at NASA’s Planetary Data System (https://pds.nasa.gov).

Code availability

The analysis presented in this work relies on proprietary orbit determination codes that are not publicly available. The MONTE software package is used at the Jet Propulsion Laboratory for planetary spacecraft navigation. The ORACLE orbit determination filter was developed at Sapienza University of Rome under contract with the Italian Space Agency.

References

23. Available at the web page **https://ssd.jpl.nasa.gov**

24. Mariotti, G. & Tortora, P. Experimental validation of a dual uplink multifrequency dispersive noise calibration scheme for deep space tracking, *Radio Sci.,* **48**, 1-7 (2013).

25. Delamere, P. A. & Bagenal, F. Modeling variability of plasma conditions in the Io torus. *J. Geophys. Research*: Space Phys. **108,** A7 (2003).

Extended data legends

Table ED1. Characteristics of perijove passes PJ3 and PJ6 used in the gravity solution. Altitude refers to the oblate planet. NON (negative orbit normal) to Earth is the angle between the opposite of the orbit normal and the Earth direction. Longitude at equator crossing refers to System III.

Table ED2. Consider covariances (3□) when a tesseral field corresponding to a flow depth of 380 km is added to the estimated zonal field in Table 1. Gravity fields generated by larger depths of the tesseral flow would produce signatures in the Doppler residuals[21].

Figure ED1. Range rate residuals. Two-way range rate residuals (integrated over 60 s) for the Ka-band pericenter passes PJ3 and PJ6. The rms value is 0.015 mm/s for both passes. The sky frequencies were obtained from the radio science open loop receiver.

Figure ED2. **Frequency stability**. Allan deviation of relative frequency shift for the Ka-band pericenter passes PJ3 and PJ6. The slopes are roughly consistent with a white frequency noise (dashed line).

Figure ED3. **Gravity harmonic signatures**. Range rate signals from J_3, J_5, J_7 and J_9 gravity harmonics for PJ3 and PJ6. The smaller signal in PJ6 is due to a less favourable projection of the spacecraft velocity along the Earth-Jupiter line of sight (the angle between the Juno orbit normal and the line of sight was 19.2° in PJ3 and 15.1° in PJ6). By comparison, the range rate noise at 60 s is 0.015 mm/s in both passes.

Figure ED4. **Io torus effects on J_3-J_5 estimation**. Estimation biases on J_3 and J_5 due to calibration errors of the Io torus path delay variation (cyan dots) in a Monte Carlo (MC) simulation of the Juno PJ3-PJ6 gravity experiment. The calibration errors are compared to the estimated 3σ uncertainty ellipses of the target solution (black), obtained without the Io torus, and the solutions obtained using X- (red) and Ka-band data only (blue). The estimation bias on J_3 is about 3σ if X-band data are used. Ka-band data or dual-link calibration reduce the bias to less than 1σ.

Figure ED5. **Io torus effects on** J_2-J_4 **estimation** Estimation biases on J_2 and J_4 from the Monte Carlo simulation as in Fig. 1. The estimation bias on J_2 and J_4 is larger than 4σ if X-band data are used, while using Ka-band or plasma calibrated data it reduces to less than 1σ.

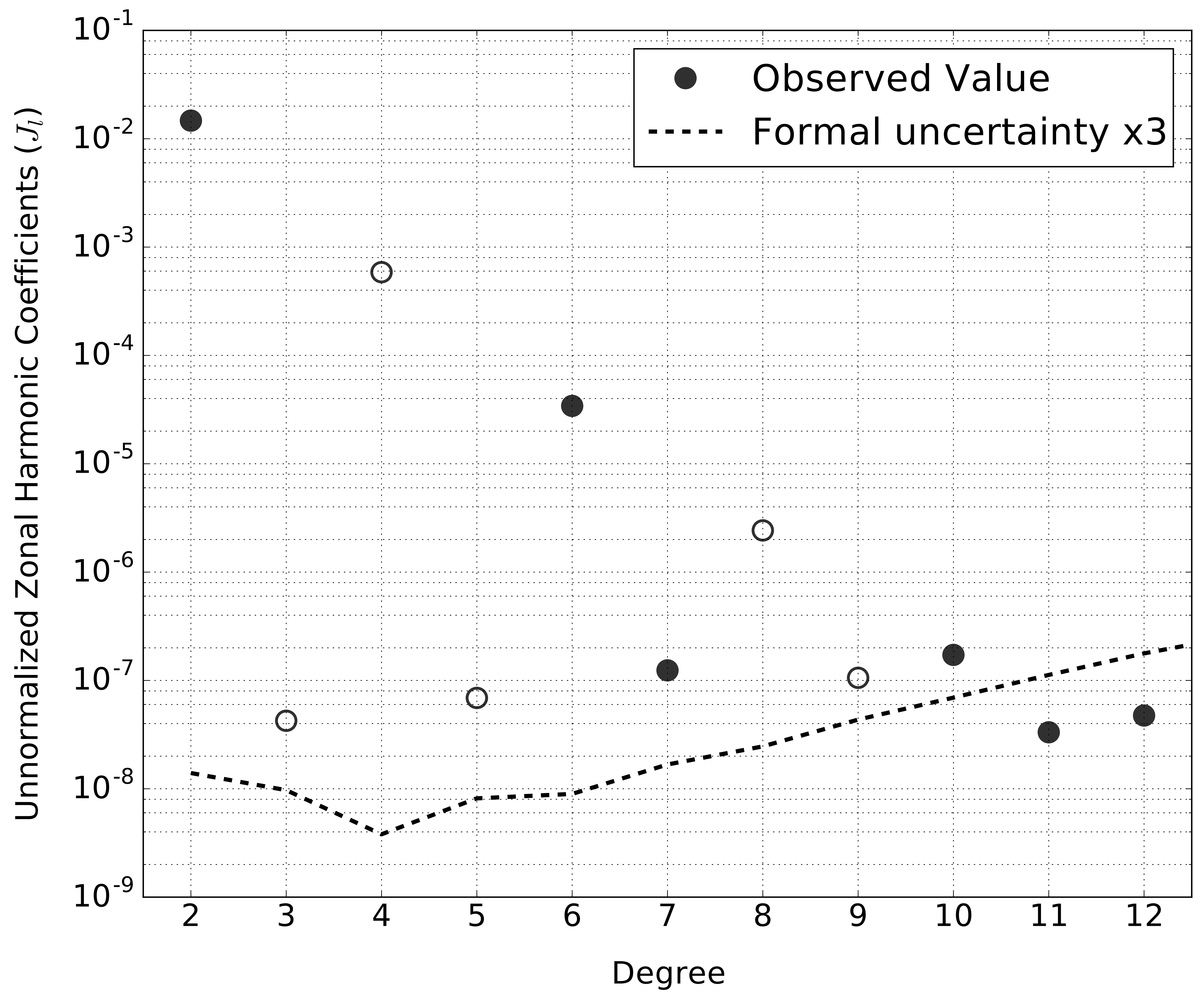

Observed Value
Formal uncertainty x3
Unnormalized Zonal Harmonic Coefficients (J_l)
10^{-1}
10^{-2}
10^{-3}
10^{-4}
10^{-5}
10^{-6}
10^{-7}
10^{-8}
10^{-9}
2
3
4
5
6
7
8
9
10
11
12
Degree

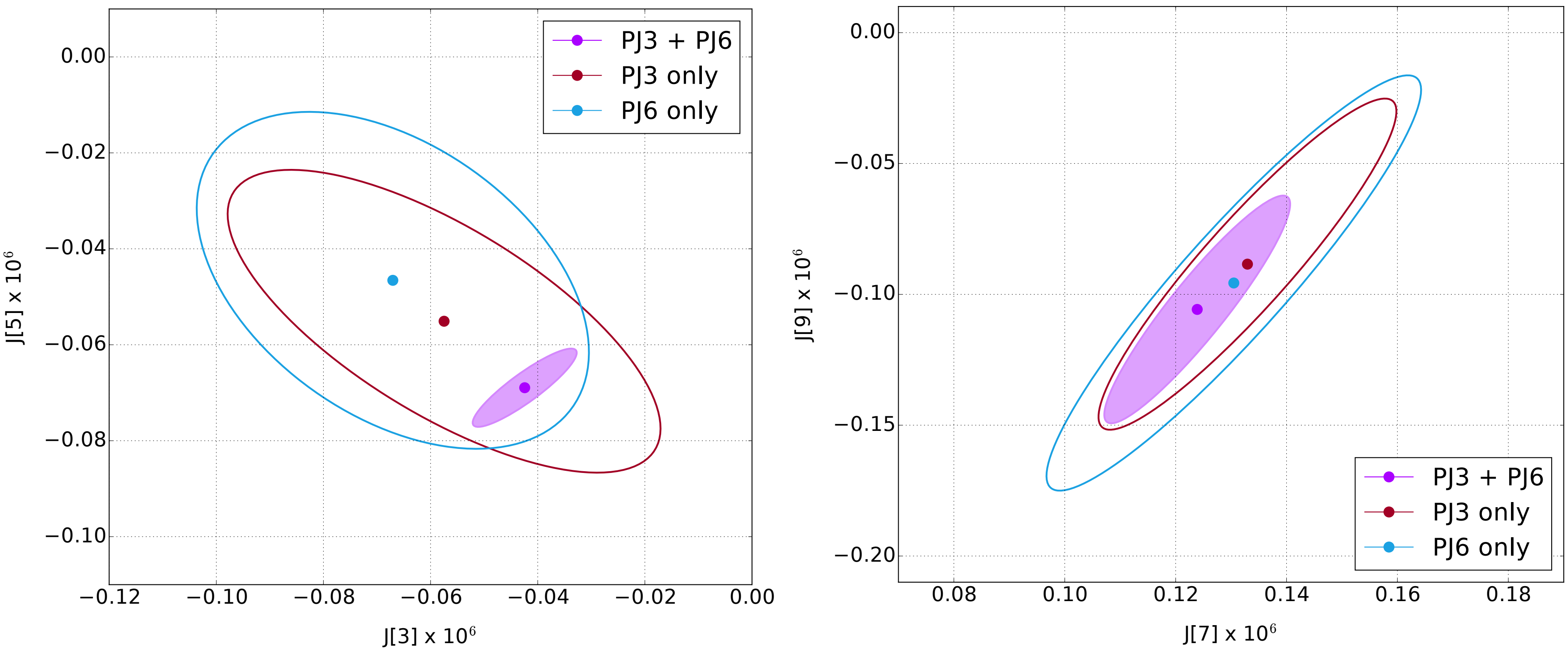
PJ3 + PJ6
PJ3 only
PJ6 only
J[5] x 10⁶
J[3] x 10⁶
0.00
−0.02
−0.04
−0.06
−0.08
−0.10
−0.12
−0.10
−0.08
−0.06
−0.04
−0.02
0.00
J[9] x 10⁶
J[7] x 10⁶
0.00
−0.05
−0.10
−0.15
−0.20
0.08
0.10
0.12
0.14
0.16
0.18

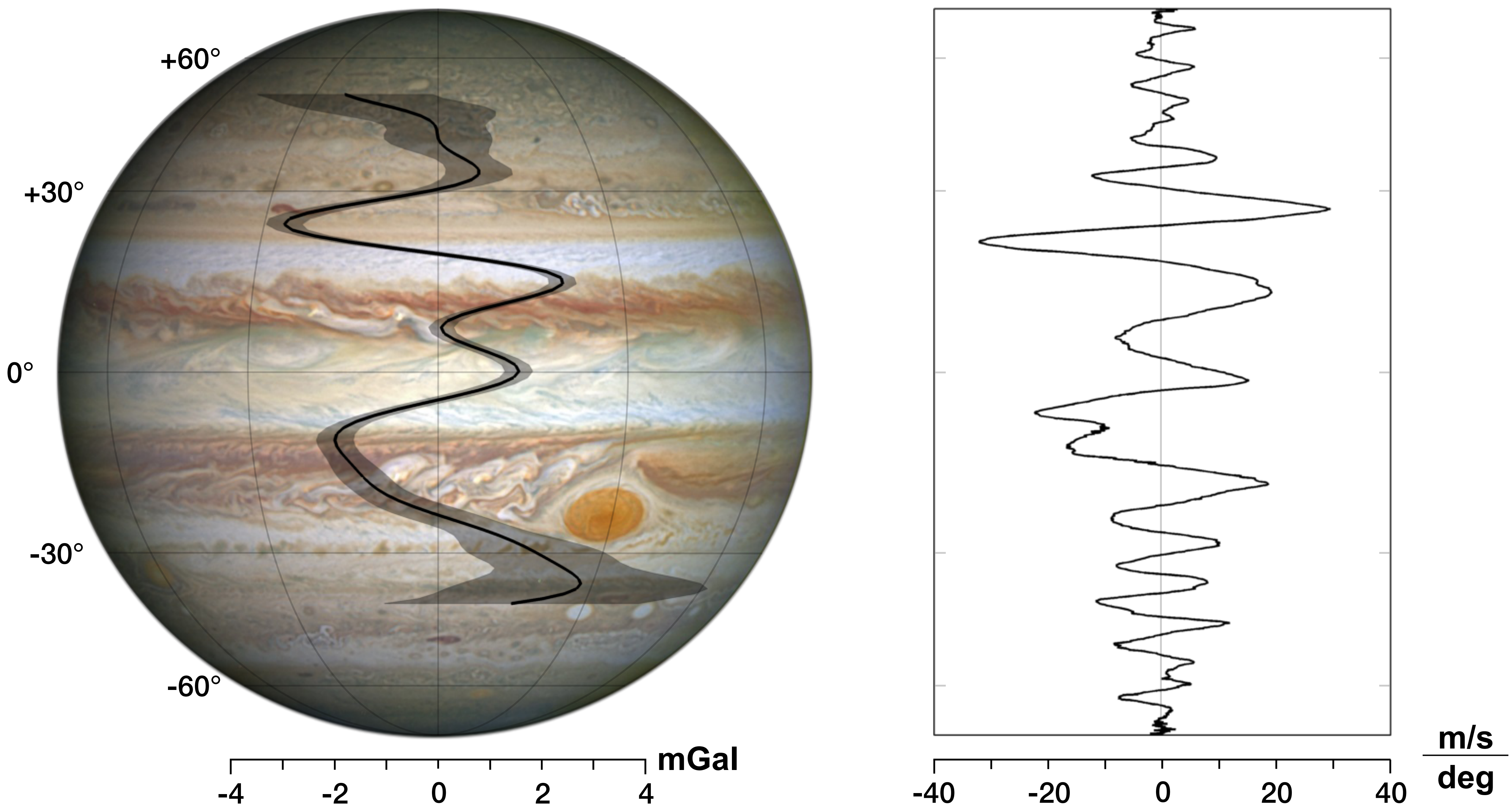
+60°
+30°
0°
-30°
-60°
-4
-2
0
2
4
mGal
-40
-20
0
20
40
m/s
deg

	Value	Uncertainty
J_2 (x10^6)	14696.572	0.014
C_{21} (x10^6)	-0.013	0.015
S_{21} (x10^6)	-0.003	0.026
C_{22} (x10^6)	0.000	0.008
S_{22} (x10^6)	0.000	0.011
J_3 (x10^6)	-0.042	0.010
J_4 (x10^6)	-586.609	0.004
J_5 (x10^6)	-0.069	0.008
J_6 (x10^6)	34.198	0.009
J_7 (x10^6)	0.124	0.017
J_8 (x10^6)	-2.426	0.025
J_9 (x10^6)	-0.106	0.044
J_{10} (x10^6)	0.172	0.069
J_{11} (x10^6)	0.033	0.112
J_{12} (x10^6)	0.047	0.178
k_{22}	0.625	0.063
RA (deg)	268.0570	0.0013
Dec (deg)	64.4973	0.0014